

RSC Advances



This is an *Accepted Manuscript*, which has been through the Royal Society of Chemistry peer review process and has been accepted for publication.

Accepted Manuscripts are published online shortly after acceptance, before technical editing, formatting and proof reading. Using this free service, authors can make their results available to the community, in citable form, before we publish the edited article. This *Accepted Manuscript* will be replaced by the edited, formatted and paginated article as soon as this is available.

You can find more information about *Accepted Manuscripts* in the [Information for Authors](#).

Please note that technical editing may introduce minor changes to the text and/or graphics, which may alter content. The journal's standard [Terms & Conditions](#) and the [Ethical guidelines](#) still apply. In no event shall the Royal Society of Chemistry be held responsible for any errors or omissions in this *Accepted Manuscript* or any consequences arising from the use of any information it contains.

Scalable Synthesis and Surface Stabilization of Li_2MnO_3 NWs as High Rate Cathode Materials for Li-Ion Batteries

Venkat Kalyan Vendra^{a,b}, Tu Quang Nguyen^{a,b}, Arjun KumarThapa^b, Jacek B. Jasinski^b,
Mahendra K. Sunkara^{*a,b}

^a Department of Chemical Engineering, University of Louisville, Louisville, KY 40292, USA.

^b Conn Center for Renewable Energy Research, University of Louisville, Louisville, KY 40292, USA.

* Corresponding author's email: mahendra@louisville.edu

Abstract

Li_2MnO_3 nanowires (NWs) are synthesized using a scalable two-step process involving a solvo-plasma technique, utilizing inexpensive precursors such as commercially available MnO_2 microparticle powders and KCl, followed by a solid state lithiation process. Lithium manganese oxide (Li_2MnO_3) nanowires exhibited high capacity retention of 120 mAh/g in the 2V– 4.5V voltage window even at high C-rates such as 20 C. The specific capacity of the Li_2MnO_3 NWs gradually increased with cycling and subsequently stabilized. Further, the Li_2MnO_3 NW cathodes exhibited no loss in the capacity for 100 cycles with close to 100 % coulombic efficiency. Most importantly, single crystalline Li_2MnO_3 nanowires with short transport length scales for Li, O and Mn atoms along the radial direction allow for the formation of thick and conformal LiMn_2O_4 shell resulting in increased capacity, excellent capacity retention and high coulombic efficiencies.

Keywords: Solvo-plasma, Li_2MnO_3 , layered lithium rich oxides, cathode, nanowire powders, Li ion batteries

Layered lithium rich manganese oxides, such as Li_2MnO_3 and its related alloys, have attracted significant interest due to their potential for achieving high capacity (~ 280 mAh/g) and energy density (~ 1000 Wh/Kg) when compared to the commercially available cathodes for Li ion batteries.¹ Slow diffusion of lithium ions, voltage loss during cycling and low faradaic efficiencies have been identified as the major scientific barriers associated with the utilization of layered lithium rich manganese oxides in Li ion batteries.^{1, 2} The use of 1-D nanostructures such as nanowires (NWs) can provide an attractive solution to overcome these barriers. A few reports have already reported the advantages of using NW architectures for lithium manganese oxides. In the case of spinels such as LiMn_2O_4 , Cui and coworkers reported that using ultrathin single crystalline nanowires can result in fast Li ion transport and facile strain relaxation during cycling, leading to improved kinetics and good capacity retention at high charge-discharge rates.³ In particular, they found that phase change associated with the transformation of cubic LiMn_2O_4 to tetragonal $\text{Li}_2\text{Mn}_2\text{O}_4$, owing to Jahn-Teller effect, occurs without any loss of capacity in thin single crystalline NWs.

In spite of all these interesting properties of NWs, the large scale synthesis of NWs of manganese related oxides is still a challenge. Many reports on the synthesis of 1-D nanomaterials of manganese oxides have utilized hydrothermal^{4, 5}, solvothermal³ and template based methods⁶ that are very difficult to scale up due to the long reaction times scales,^{7, 8} low yields, and the use of expensive precursors. For instance, the commonly used hydrothermal method for making 1D nanostructures of manganese oxide requires at least 12 h of autoclaving.^{3, 9} We have recently reported a scalable approach, called solvo-plasma process, for making titanium dioxide NWs. The process involves the exposure of inexpensive precursors such as titania nanoparticle powders and alkali metal salts to an atmospheric microwave plasma.¹⁰ The reaction times scales

in this process are very short from about a few seconds to 5 minutes. In this paper, we report a similar scheme for the large-scale synthesis of manganese oxide nanowires followed by their conversion to lithium manganese oxide by solid state alloying with lithium hydroxide.

Apart from developing scalable methods for synthesis, achieving high coulombic efficiency has been another major challenge with Li_2MnO_3 . The Li extraction process from Li_2MnO_3 has been found to occur by two competing processes, the first involves the removal of oxygen and the second involves ion-exchange of Li^+ in the lattice with H^+ from the electrolyte.¹¹ The initial discharge process was shown to involve a small loss of oxygen anions from the lattice to balance the charge associated with Li^+ extraction. Subsequent Li extraction is shown to proceed with Li^+ ions exchanging with H^+ ions from the electrolyte during discharge and exchange of H^+ ions with Li^+ ions during charging. The repeated shearing of the layers containing oxygen atoms has been shown to result in structural degradation and subsequent capacity loss in the case of Li_2MnO_3 .¹² A prior report indicated a coulombic efficiency of 50 % for Li_2MnO_3 NWs and 30 % for bulk Li_2MnO_3 particles.² Further, achieving minimum capacity loss at high C-rates is a crucial requirement for the commercial viability of electrode materials for Li ion batteries. Li_2MnO_3 NWs prepared in this work showed no capacity fade even at 20 C discharge rate, with close to 100 % coulombic efficiency. The reasons for such high capacity retention are explained by characterizing the Li_2MnO_3 NW electrodes that have been tested for several charge and discharge cycles.

The large-scale synthesis of Li_2MnO_3 NWs is schematically illustrated in Figure 1. The process involves two steps: (i) the synthesis of manganese oxide nanowires by solvo-plasma technique followed by (ii) solid state alloying with lithium hydroxide. The synthesis of the MnO_2 NWs by the solvo-plasma technique is detailed in the supporting information. Briefly, the

process involves the deposition of micron sized MnO_2 powder mixed with KCl on a stainless steel foil followed by the exposure of the foil to an atmospheric microwave plasma flame. The powder on the stainless foil is scraped off, immersed in 1M HCl for an hour, rinsed with deionized water several times and annealed at 200 °C to produce MnO_2 NWs. These MnO_2 NWs are subsequently alloyed with LiOH at 480°C to form Li_2MnO_3 NWs. The Li_2MnO_3 NWs have an average diameter of 50 nm and lengths close to a 1 μm . The as-synthesized Li_2MnO_3 NWs are found to be single crystalline and have a d-spacing of 0.32 nm (Figure 2b) which is close to the d-spacing value of 0.317 nm for the (022) plane of Li_2MnO_3 NWs according to the PDF# 00-018-0737.

Prior to testing the Li_2MnO_3 NWs, we evaluated the performance of the MnO_2 NWs as cathodes in Li ion batteries. The electrochemical testing of MnO_2 NWs shows severe capacity loss with cycling. This can be attributed to slow kinetics of Li intercalation and deintercalation and poor conductivity of MnO_2 NWs (Supporting information, Figure S2). In contrast to MnO_2 NWs, the Li_2MnO_3 NWs showed faster Li intercalation and deintercalation kinetics as indicated from closer separation of the Li insertion and extraction peaks in the cyclic voltammogram of Li_2MnO_3 NWs shown in Figure 2. The cathodic peaks at 4.05 V and 2.7 V correspond to Li intercalation while the anodic peaks at 3.1 V and 4.1 V correspond to Li de-intercalation respectively. The redox peaks close to 3 V can be attributed to the phase transformation of the layered structure to a spinel structure.^{2, 13} Although the oxidation state of Mn in Li_2MnO_3 is expected to +4 in theory, recent reports indicated the presence of both +4 and +3 states of Mn in Li_2MnO_3 prepared at low temperatures (< 800 °C). Our prior work showed that oxygen vacancies are typically present in metal oxide nanowires.¹⁴ The +3 oxidation state for Mn could also be

caused by the oxygen vacancies present in Li_2MnO_3 NWs. Hence, the peaks observed at 4.05 V and 4.1 V can be attributed to the $\text{Mn}^{+3}/\text{Mn}^{+4}$ redox reaction in Li_2MnO_3 .^{13, 15}

The electrochemical performance and cycling stability of the Li_2MnO_3 NWs was evaluated by determining the charge-discharge characteristics using a coin cell configuration. Figure 3 shows charge and discharge voltage profile for Li_2MnO_3 NWs. It should be noted that our coin cell testing has been done at relatively good cell loading of 5 mg/cm^2 of active material. The cycling was carried out in the 2 V to 4.5 V range. The pseudo plateau region observed at 4.1 V is due to the lithium extraction from LiMn_2O_4 spinel phase. This plateau is not clearly seen in the first charge-discharge cycle, but becomes more dominant in the subsequent charge-discharge cycles indicating that LiMn_2O_4 is formed in the first few cycles of lithiation and delithiation. The diagonal shape of the voltage profile between 4 V and 3 V is similar to that of Li_xMnO_2 phase and the plateau region at 3 V has been attributed to lithium insertion/extraction in the octahedral sites of the spinel $\text{Li}_{1+x}\text{Mn}_2\text{O}_4$ phase.¹⁶ Li_2MnO_3 NWs showed a low initial capacity of $\sim 80 \text{ mAh g}^{-1}$ at 1C and $\sim 90 \text{ mAh g}^{-1}$ at 5C, which is much lower than the theoretical capacity of Li_2MnO_3 of 280 mAh g^{-1} . This is due to Li_2MnO_3 being electrochemically inactive when cycled below 4.5V.^{17, 18}

In order to understand the different structural transformations occurring in the Li_2MnO_3 NWs, two different electrodes were discharged to 3.5 V and 2 V and were characterized using XRD (Figure 4) and HRTEM (Figure 5). The XRD pattern of the as-synthesized Li_2MnO_3 NWs is shown in Figure 4a, and matches very well with the XRD pattern for phase pure Li_2MnO_3 (PDF # 00-018-0737). No diffraction peaks from LiMn_2O_4 were observed. Further, no plateau was observed in the 4 V region in first charge cycle of Figure 3, indicating negligible amount of LiMn_2O_4 in the as-synthesized sample. The XRD of the sample discharged to 3.5 V showed

Li_2MnO_3 as the dominant phase and remaining few peaks could be indexed to LiMn_2O_4 , $\text{Li}_{0.78}\text{Mn}_{0.85}\text{O}_2$ and LiMn_3O_4 . When the sample was further discharged to 2 V, Li_2MnO_3 remained as the dominant phase and diffraction peaks corresponding to tetragonal $\text{Li}_2\text{Mn}_2\text{O}_4$ phase were also observed. The phase transition from cubic LiMn_2O_4 to tetragonal $\text{Li}_2\text{Mn}_2\text{O}_4$ has been reported to occur in LiMn_2O_4 samples discharged below 3.5 V due to Jahn-Teller distortion effect.^{3, 19}

To investigate the spatial location of the different phases in the nanowire, HRTEM analysis was performed on the samples. Figure 5 shows HRTEM images of sample discharged to 3.5 V and 2 V respectively. The d-spacing of 0.36 nm (Figure 5c) corresponds to the (111) plane of Li_2MnO_3 . Analysis of the XRD patterns (Figure 4) and the d-spacing of 0.47 nm observed in HRTEM images (Figures 5 and 6) indicates the presence LiMn_2O_4 spinel present on the shell of the nanowires. Large d-spacings of 0.92 nm were also observed in the HRTEM images of a few Li_2MnO_3 NWs discharged to 2 V, indicating the extraction of lithium and oxygen from the core of the NWs. The d-spacing of 0.92 nm is in close agreement with the layered structure compound with composition $(\text{Li}_2\text{O})_{0.12} \text{MnO}_2$. These results suggest core-shell architecture of layered Li_2MnO_3 core covered with a polycrystalline shell of LiMn_2O_4 . Figure 6 shows HRTEM images of Li_2MnO_3 NWs discharged to 2V. Figure 6a shows a Li_2MnO_3 core - LiMn_2O_4 shell nanowire. Basing on the average thickness of the shell layer and the densities of core (density of Li_2MnO_3 is 3.896 g/cc [PDF # 01-027-3120]) and shell materials (density of LiMn_2O_4 is 4.233 g/cc [PDF # 01-070-3120]), we estimated the weight % of LiMn_2O_4 to be 70.1 % when the core is still in the form of Li_2MnO_3 . When the core is depleted of lithium and oxygen, i.e. in the form of $(\text{Li}_2\text{O})_x \text{MnO}_2$, the weight % of the LiMn_2O_4 shell is calculated to be around 92.6 % The density of $(\text{Li}_2\text{O})_x \text{MnO}_2$, where x is small, is approximated to the density of $(\text{Li}_2\text{O})_{0.12} \text{MnO}_2$

which 4.221 g/cc [PDF # 01-074-8725]. The high volume fraction of the spinel shell accounts for observed high weight % spinel in the nanowires. After 40 cycles (LiMn_2O_4 shell = 75.8 Wt % from Table S1 in supporting information), the capacity starts to stabilize to a constant value (Figure 3b). Hence, the LiMn_2O_4 shell thickness after 40 cycles, calculated as 14 nm (for an NW of diameter 56 nm), could be regarded as the minimum shell thickness required for a stable capacity retention. The weight % of spinel and layered phases calculated from TEM analysis are based on the shell thickness on a limited number of nanowires. To calculate an average thickness of the spinel shell, a previously reported calculation involving the first cycle discharge capacity was used (See Supporting information Table S1).¹⁶ Based on these calculations, the average weight % of LiMn_2O_4 after 100 cycles is estimated as 85 %. Details of the calculation are indicated in the supporting information. Figure 7 shows the SAED patterns of the Li_2MnO_3 NWs discharged to 3.5 V (Figure 7a) and 2 V (Figure 7b). The SAED patterns were analyzed by the rotational average method. The peaks positions for different lithium manganese oxide compounds are also indicated for comparison. The analysis indicated that the sample discharged to 3.5 V showed peaks corresponding to LiMn_2O_4 and Li_2MnO_3 phases. The sample discharged to 2 V indicated peaks corresponding to $\text{Li}_2\text{Mn}_2\text{O}_4$, Li_2MnO_3 and $(\text{Li}_2\text{O})_{0.12}\text{MnO}_2$. The SAED phase analysis is in agreement with the observations from lattice spacing measurement from HRTEM shown in Figure 5 and the XRD patterns shown in Figure 4.

Formation of spinel phases on layered Li rich compounds such as Li_2MnO_3 have been observed to enhance the cycling stability. For example, an AlF_3 coating on Li_2MnO_3 has been reported to exhibit improved capacity retention due to formation of a spinel phase on surface of cathode material.²⁰ Chen et al. reported that a spinel $\text{Li}_{1+x}\text{Mn}_2\text{O}_4$ layer formed by dip coating the $\text{Li}_{1.2}\text{Mn}_{0.6}\text{Ni}_{0.2}\text{O}_2$ microparticles enhanced the capacity retention by acting as a barrier for erosion

of the layered material into the electrolyte while still permitting fast ion transport through the 3D Li ion transport channels in the spinel.^{21,22} It has been shown that Li delithiation results in a surface reconstruction of the layered lithium metal oxide, causing the transition metal atoms to migrate to the lithium sites resulting in the formation of the spinel phase.^{23, 24} Further, surface reconstruction has been shown to add a significant charge transport resistance with some initial capacity loss. However, it is interesting to note that the opposite effect is observed in our case, i.e., the capacity increases with the cycling and then stabilizes at a constant value. In the case of Li_2MnO_3 NWs, the single crystalline core could assist in the strain relaxation associated with the surface phase transitions of the spinel phase without any capacity loss. Figure 8 shows the proposed mechanism of surface reconstruction and phase transformation in Li_2MnO_3 NWs. During the first charge cycle, where Li deintercalation occurs, the Li ions along with oxygen anions diffuse outwards from the core of the NW. An indirect evidence for the Li and oxygen atoms diffusing out is the wide d-spacing observed in our HRTEM images (Figures 5b and 6c). The oxygen anions then reduce the valence of Mn atoms from +4 to +3 and Li^+ ions to Li atoms. The Li, Mn and O atoms reaching the surface of the nanowire react to nucleate and grow LiMn_2O_4 shell around the nanowire during the first discharge cycle. No peaks or plateaus are observed in our first charge process up to 4.5 V, indicating that the oxygen atoms migrate to the surface rather than oxygen gas being evolution in the first cycle. In addition, there is clear evidence for oxygen evolution when the cells are charged up to 4.8 V (Figure S5 of Supporting Information). Our reaction mechanism is also supported by the findings of Chen and coworkers who used EELS spectroscopy and high resolution S-TEM to demonstrate that the oxidation state of Mn changes from +4 to +3 during cycling and also showed the formation of spinel phase on the surface of layered lithium manganese oxide particles.²⁴ The nucleation and growth of spinel

during the first cycle is responsible for the low coulombic efficiency in the first cycle as some of the charge is utilized for the phase transformation to the spinel besides carrying out the lithiation/delithiation reaction.

During lithiation or discharge, the delithiated core changes back to Li_2MnO_3 , with a LiMn_2O_4 nanocrystalline shell on the surface of the NWs. Further lithiation (from 3.5 V to 2 V) transforms the shell from cubic LiMn_2O_4 to tetragonal $\text{Li}_2\text{Mn}_2\text{O}_4$ due to Jahn-Teller distortion effect. LiMn_2O_4 nanocrystalline shell stabilized the Li_2MnO_3 from erosion effects of the electrolyte and also contributes to a slight improvement in capacity during cycling. The single crystalline NW core allows for the phase transformation on the spinel shell to occur without any capacity fade. The single crystal core, depleted of insulating Li_2O , exhibits high conductivity allowing fast electron transport.

The increased capacity with cycling could be attributed to the formation of LiMn_2O_4 , which has been reported to exhibit higher capacity (116 mAh/g at 1 C rate)³ when compared to Li_2MnO_3 (75 mAh/g at 0.44 C)². Prior reports have shown significant capacity loss associated with voltage plateau at 3 V due to the difficulty in reversing the tetragonal phase back to the cubic phase (caused by Jahn-Teller distortion) and significant strain on the lattice during this phase transformation.^{25, 26} However no capacity fade associated with this transition is observed in our system. This could be due to the facile stress relaxation of the extremely thin LiMn_2O_4 layer on a single crystal NW. The small transport length scales for Li ions, oxygen and manganese atoms along the diameter single crystal nanowires allow for the thick LiMn_2O_4 spinel shell (15-20 nm) formation on the surface resulting in high coulombic efficiency and excellent capacity retention at high C rates. In case of polycrystalline nano/microparticles of Li_2MnO_3 , the formation of LiMn_2O_4 is either very thin (<2 nm)²³ or non-conformal^{27, 28} leading to poor

protection Li_2MnO_3 especially at high C rates. This makes single crystalline Li_2MnO_3 nanowires a unique platform for surface phase transformation to obtain thicker and more conformal shell of LiMn_2O_4 . The experimental observations by Meng et al. also support our argument of oxygen migration when the Li_2MnO_3 cells are charged only until 4.5 V.²³

An important requirement for a Li ion battery cathode is to have high capacity retention when the electrode is cycled at high C rates. To illustrate the high rate capability of the Li_2MnO_3 NWs, the charge-discharge testing was performed at different C rates. Figure 9 represents the cycling performance of Li_2MnO_3 NW cathode at different C-rates and shows the capacity drop from 135 mAh/g to 125 mAh/g, 120 mAh/g, 110 mAh/g as the C-rate increased from 1C to 5C, 10C and 20C, respectively. The capacity increased back to 135 mAh/g when the electrode is cycled at 1C rate indicating good reversibility and high rate capacity of Li_2MnO_3 NWs. The fast kinetics of Li intercalation and de-intercalation in the Li_2MnO_3 NWs with a spinel phase protective coating are responsible for the observed high rate capacity. Most importantly, the high scalability of the solvo-plasma method makes it possible to produce commercial scale quantities of manganese oxide nanowires for application towards Li ion batteries. Furthermore, Li_2MnO_3 NWs show potential for the use of thick electrodes because of their impressive capacity retention at high C-rates.

Conclusions

In summary, a scalable approach for synthesizing MnO_2 nanowires is demonstrated using a solvo-plasma technique. Li_2MnO_3 NWs prepared by the solid state lithiation of the MnO_2 NWs, showed high capacity retention (95.8 %) even at 20 C-rate. The formation of a spinel phase LiMn_2O_4 shell on the nanowires resulted in a gradual increase in capacity with cycling

and allowed a stable capacity to be maintained at high C-rates. The nanocrystalline LiMn_2O_4 shell layer undergoes Jahn-Teller distortion without significant capacity loss, due to facile strain relaxation properties of the nanowires. Single crystalline Li_2MnO_3 NWs provide a unique platform for facile surface phase transformation, due to small transport length scales in the radial direction, resulting in formation of thick and conformal LiMn_2O_4 protective shell on the Li_2MnO_3 NWs thereby leading to excellent capacity retention at high C rates.

Experimental

Micron sized MnO_2 powder (Alfa Aesar) and KCl (Sigma Aldrich) were mixed with water in mortar and pestle to make a paste. A thick layer (~ 100 microns) of this paste is deposited on a stainless steel substrate. The substrate is dried on a hot plate at 70°C to evaporate the water and is cooled to room temperature and subsequently exposed to an atmospheric plasma flame for 5 minutes. The details of experimental setup of the atmospheric microwave plasma reactor are described elsewhere.¹⁰ An air flow rate of 8 lpm and a plasma power of 750 W were used. The thick film was removed from the substrate while leaving a small part of it on the substrate in order to prevent contamination from stainless steel foil. The use of a stainless steel foil as the substrate was found to be better than using either quartz or sapphire substrates to make the nanowires. The resulting products on the substrate are then washed with deionized water several times to remove the unreacted salt, and then immersed in 1 M HCl for 2 hours. The remaining products are then heated to 200°C resulting in manganese oxide. For synthesis of lithium manganese oxide, the manganese oxide nanowires and lithium hydroxide (1:1 ratio) were mixed in ethanol to form a homogeneous mixture and then heated in an oven for 12 h at 480°C .

The battery testing was carried out using a coin cell configuration using an Arbin battery tester. The electrochemical characterizations were carried out using a CR2013 coin-type cell assembled in a dry argon-filled glove box. The cathode was formed by mixing 10 mg of active electrode with 3 mg of teflonized acetylene black (TAB-2) as a conducting binder. The mixture was pressed onto stainless steel mesh. The average thickness of cathode was 18-20 μm and lithium foil was used as a counter electrode separated by a porous propylene film (ADVANTEC GB-100R). The cathode was dried at 150°C for 5 h under vacuum. The electrolyte used was 1M LiPF_6 -EC: DMC (1:2). The charge-discharge measurements are carried out using a battery tester (16-channel Arbin Instrument, USA) in a voltage window of 2 V to 4.5 V. Cyclic voltammetry was performed using eDaQ e-corder and potentiostat. A loading of 5 mg/cm^2 of active material was used for all our electrodes tested in this work.

Scanning electron microscopy (SEM) was performed with a NOVA FEI scanning electron microscopy. XRD patterns were obtained with a Bruker D8 discover X-ray diffractometer. Cu K_{α} (1.549 \AA) radiation was used for obtaining the XRD patterns. Transmission electron microscopy (TEM) was performed using a Tecnai F20 FEITEM equipped with a Gatan 2002 GIF system.

Acknowledgement

The authors acknowledge Conn Center for Renewable Energy Research for experimental facilities and funding support and also acknowledge partial support from National Science Foundation (NSF EPSCoR) 1355438. The authors acknowledge Ms. Swathi Sunkara for her assistance with the manganese oxide sample preparation.

Electronic Supplementary Information

(ESI) available: Details of the synthesis and electrochemical characterization of manganese oxide nanowires, crystal structures of different phases lithium manganese oxide compounds formed during cycling are shown in the supplementary document.

References

1. H. Yu and H. Zhou, *The Journal of Physical Chemistry Letters*, 2013, **4**, 1268-1280.
2. X. Wu, H. Li, H. Fei, C. Zheng and M. Wei, *New Journal of Chemistry*, 2014, **38**, 584-587.
3. H.-W. Lee, P. Muralidharan, R. Ruffo, C. M. Mari, Y. Cui and D. K. Kim, *Nano letters*, 2010, **10**, 3852-3856.
4. F. Cheng, J. Zhao, W. Song, C. Li, H. Ma, J. Chen and P. Shen, *Inorganic chemistry*, 2006, **45**, 2038-2044.
5. X. Wang and Y. Li, *Journal of the American Chemical Society*, 2002, **124**, 2880-2881.
6. X. Wang, X. Wang, W. Huang, P. Sebastian and S. Gamboa, *Journal of Power Sources*, 2005, **140**, 211-215.
7. U. Cvelbar, *Journal of Physics D: Applied Physics*, 2011, **44**, 174014.
8. K. K. Ostrikov, U. Cvelbar and A. B. Murphy, *Journal of Physics D: Applied Physics*, 2011, **44**, 174001.
9. D. K. Kim, P. Muralidharan, H.-W. Lee, R. Ruffo, Y. Yang, C. K. Chan, H. Peng, R. A. Huggins and Y. Cui, *Nano letters*, 2008, **8**, 3948-3952.
10. V. Kumar, J. H. Kim, J. B. Jasinski, E. L. Clark and M. K. Sunkara, *Crystal Growth & Design*, 2011, **11**, 2913-2919.
11. A. D. Robertson and P. G. Bruce, *Chemistry of Materials*, 2003, **15**, 1984-1992.
12. J. Rana, M. Stan, R. Kloepsch, J. Li, G. Schumacher, E. Welter, I. Zizak, J. Banhart and M. Winter, *Advanced Energy Materials*, 2014, **4**.
13. S. F. Amalraj, D. Sharon, M. Talianker, C. M. Julien, L. Burlaka, R. Lavi, E. Zhecheva, B. Markovsky, E. Zinigrad and D. Kovacheva, *Electrochimica Acta*, 2013, **97**, 259-270.
14. B. D. Chernomordik, H. B. Russell, U. Cvelbar, J. B. Jasinski, V. Kumar, T. Deutsch and M. K. Sunkara, *Nanotechnology*, 2012, **23**, 194009.
15. S.-H. Park, Y. Sato, J.-K. Kim and Y.-S. Lee, *Materials chemistry and physics*, 2007, **102**, 225-230.
16. S.-H. Park, Y. Sato, J.-K. Kim and Y.-S. Lee, *Materials chemistry and physics*, 2007, **102**, 225-230.
17. L. Xiong, Y. Xu, T. Tao, J. Song and J. B. Goodenough, *Journal of Materials Chemistry*, 2012, **22**, 24563-24568.
18. M. M. Thackeray, S.-H. Kang, C. S. Johnson, J. T. Vaughey, R. Benedek and S. Hackney, *Journal of Materials Chemistry*, 2007, **17**, 3112-3125.
19. J. Choa and M. M. Thackeray, *Journal of The Electrochemical Society*, 1999, **146**, 3577-3581.
20. Y. K. Sun, M. J. Lee, C. S. Yoon, J. Hassoun, K. Amine and B. Scrosati, *Advanced Materials*, 2012, **24**, 1192-1196.
21. F. Wu, N. Li, Y. Su, H. Shou, L. Bao, W. Yang, L. Zhang, R. An and S. Chen, *Advanced Materials*, 2013, **25**, 3722-3726.
22. F. Wu, N. Li, Y. Su, L. Zhang, L. Bao, J. Wang, L. Chen, Y. Zheng, L. Dai and J. Peng, *Nano letters*, 2014.
23. B. Xu, C. R. Fell, M. Chi and Y. S. Meng, *Energy & Environmental Science*, 2011, **4**, 2223-2233.

24. F. Lin, I. M. Markus, D. Nordlund, T.-C. Weng, M. D. Asta, H. L. Xin and M. M. Doeff, *Nature communications*, 2014, **5**.
25. F. Jiao, J. Bao, A. H. Hill and P. G. Bruce, *Angewandte Chemie International Edition*, 2008, **47**, 9711-9716.
26. D. A. Robertson, Armstrong, A. Robert; Bruce, P.G., *Chem. Mater.*, 2001, **13**, 2380-2386.
27. B. Song, Z. Liu, M. O. Lai and L. Lu, *Physical Chemistry Chemical Physics*, 2012, **14**, 12875-12883.
28. S. Francis Amalraj, B. Markovsky, D. Sharon, M. Talianker, E. Zinigrad, R. Persky, O. Haik, J. Grinblat, J. Lampert and M. Schulz-Dobrick, *Electrochimica Acta*, 2012, **78**, 32-39.

List of Figures

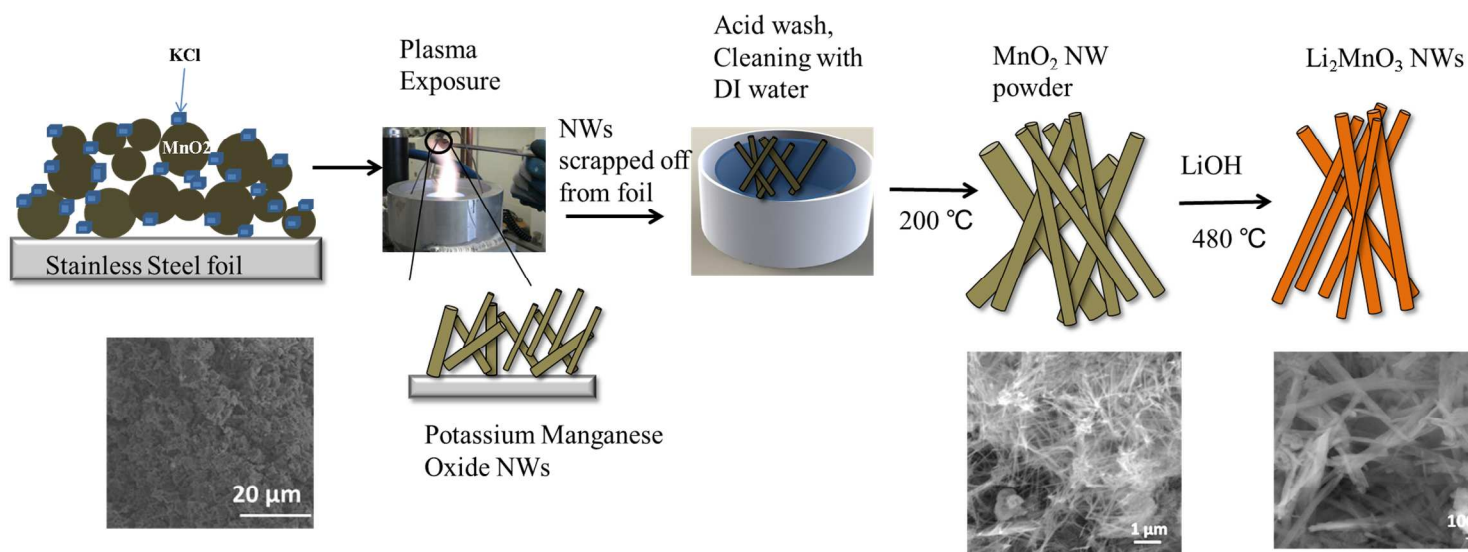


Figure 1: Schematic of the solvo-plasma process for synthesizing MnO_2 NWs followed by solid-state alloying to prepare Li_2MnO_3 NWs

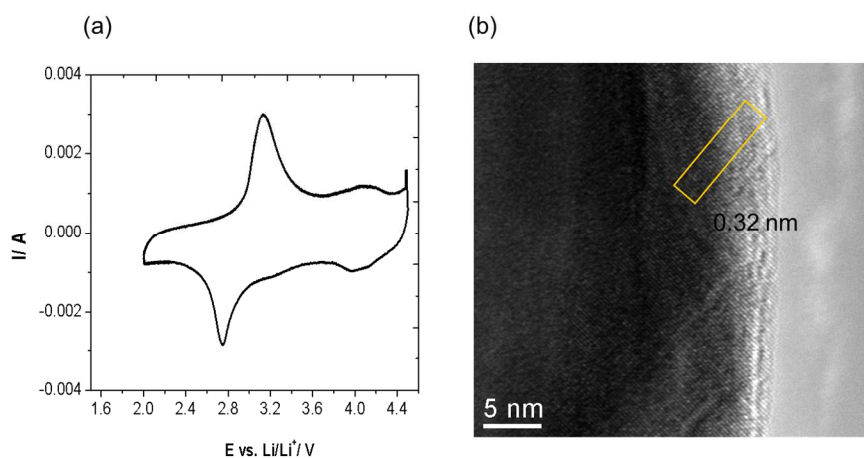


Figure 2. Cyclic voltammogram of Li_2MnO_3 NWs at a scan rate of 1 mV/s (b) HRTEM image of single crystalline Li_2MnO_3 NWs.

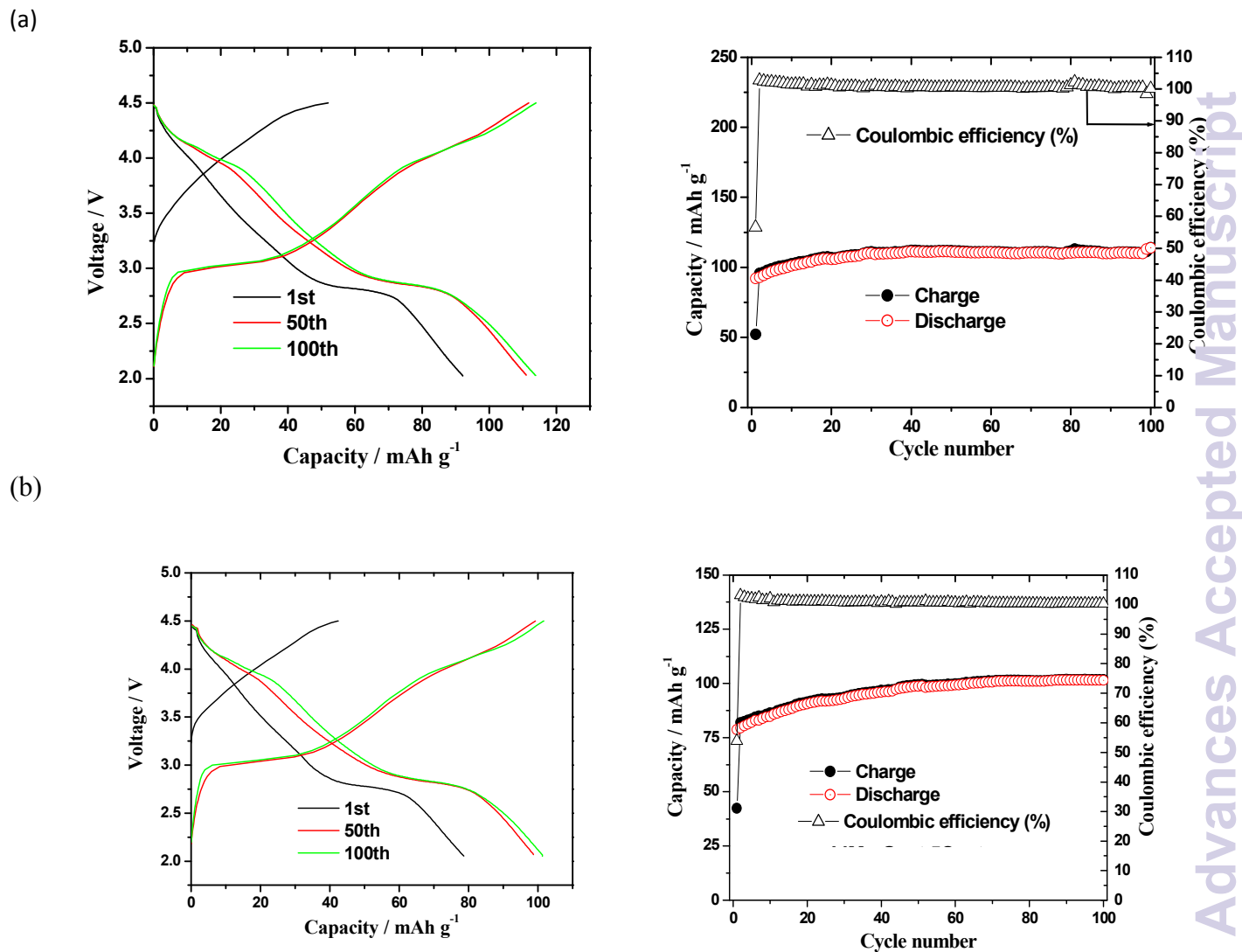


Figure 3. Charge-discharge capacity curves and cycleability of Li_2MnO_3 NWs at (a) 1C-rate and (b) at 5 C-rate respectively.

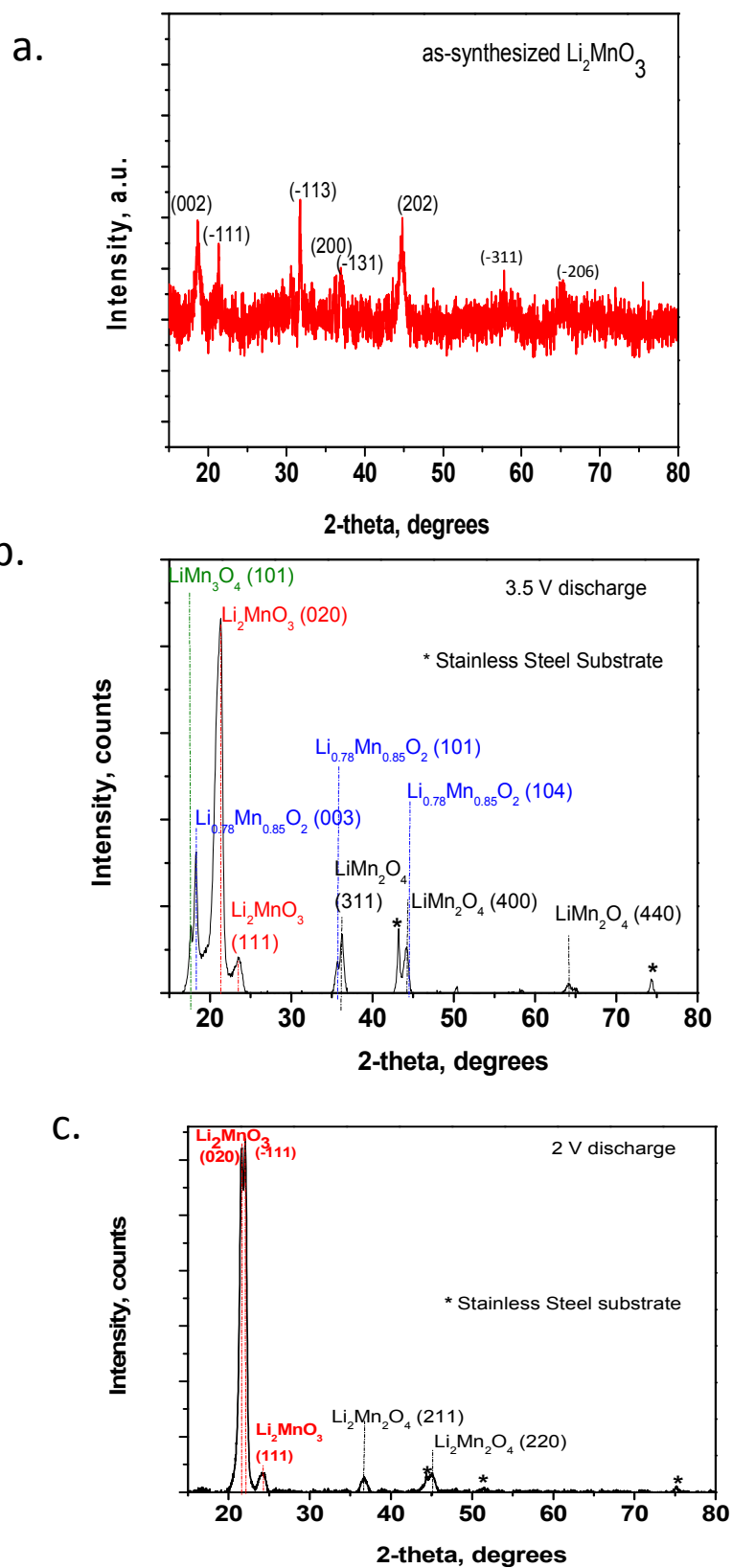


Figure 4. XRD of (a) as-synthesized Li_2MnO_3 nanowires (b) Li_2MnO_3 NWs discharged to 3.5 V and (c) Li_2MnO_3 NWs discharged to 2 V.

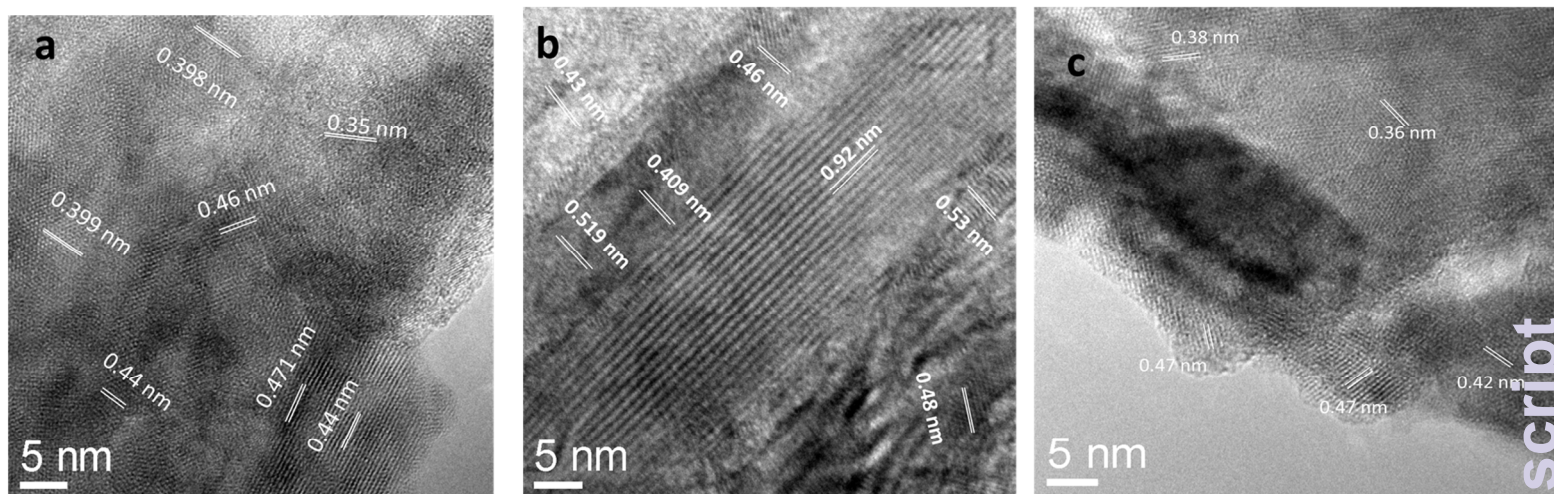


Figure 5. (a) & (b) HRTEM images of Li_2MnO_3 NWs discharged to 2 V and (c) HRTEM image of Li_2MnO_3 NW discharged to 3.5 V

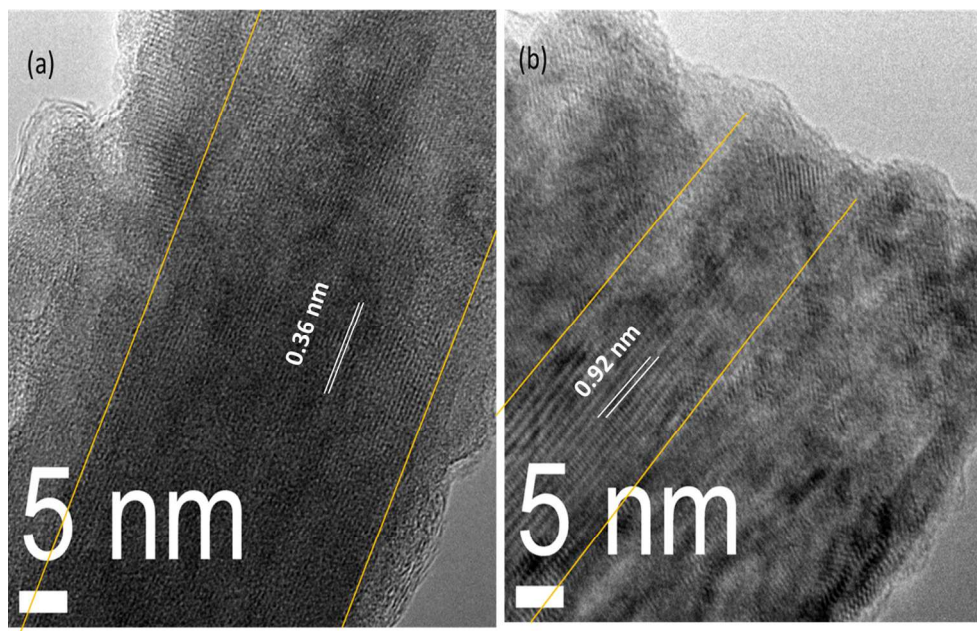


Figure 6. HRTEM images showing the a polycrystalline shell along Li_2MnO_3 NWs discharged to 2 V.

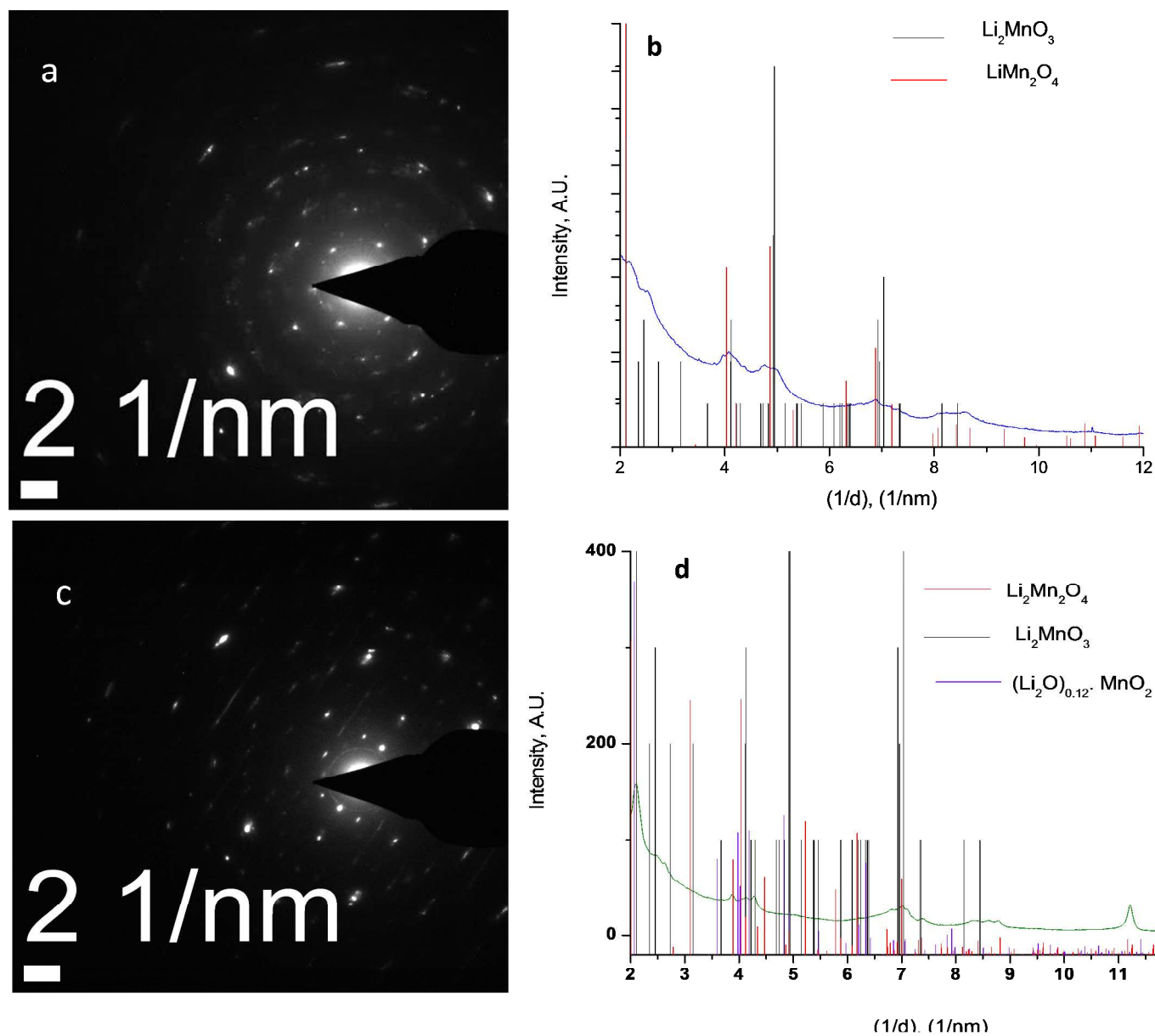


Figure 7. (a) and (c) depict the SAED pattern of the sample discharged to 3.5 V and 2V respectively. (b) and (d) show the rotational average analysis of these SAED patterns respectively.

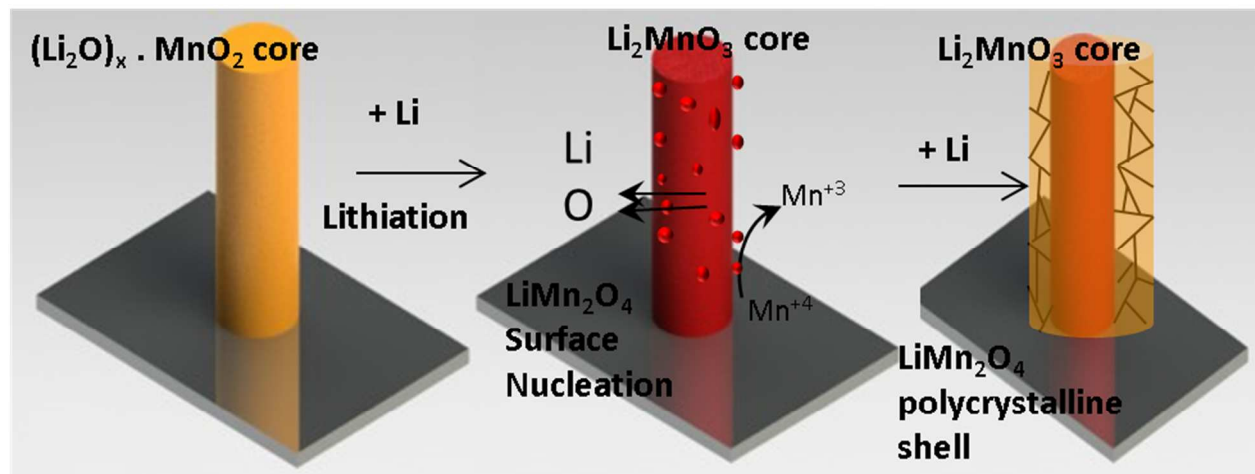


Figure 8. Schematic illustrating the formation of an LiMn_2O_4 shell on the Li_2MnO_3 NWs.

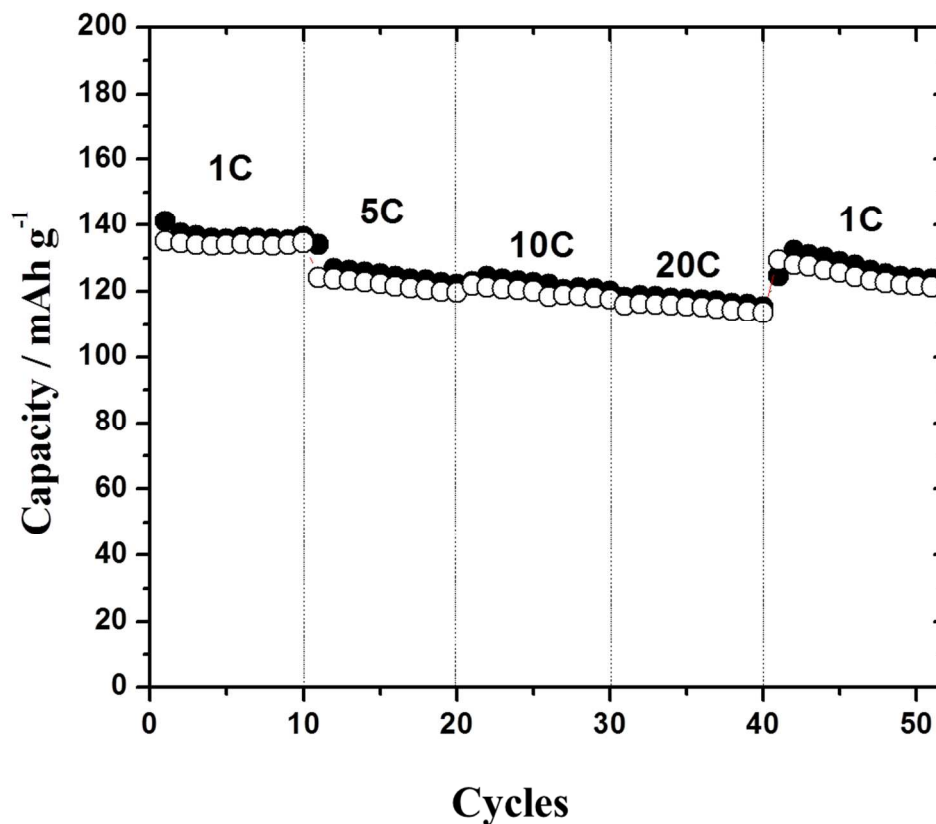


Figure 9. C-rate test of Li_2MnO_3 NWs at different current densities.

Table of contents entry

A scalable method of synthesizing Li_2MnO_3 NWs, as cathode materials for Li ion batteries, has been demonstrated and their stable performance at high rate capacity is explained basing on the formation of spinel LiMn_2O_4 shell on the Li_2O depleted Li_2MnO_3 NWs.

Keywords: Solvo-plasma, Li_2MnO_3 , layered lithium rich oxides, cathode, nanowire powders, Li ion batteries

*Venkat Kalyan Vendra^{a,b}, Tu Quang Nguyen^{a,b}, Arjun K. Thapa^b, Jacek B. Jasinski^b, Mahendra K. Sunkara^{*a,b}*

Scalable Synthesis and Surface Stabilization of Li_2MnO_3 NWs as High Rate Cathode Materials for Li-Ion Batteries

ToC Figure

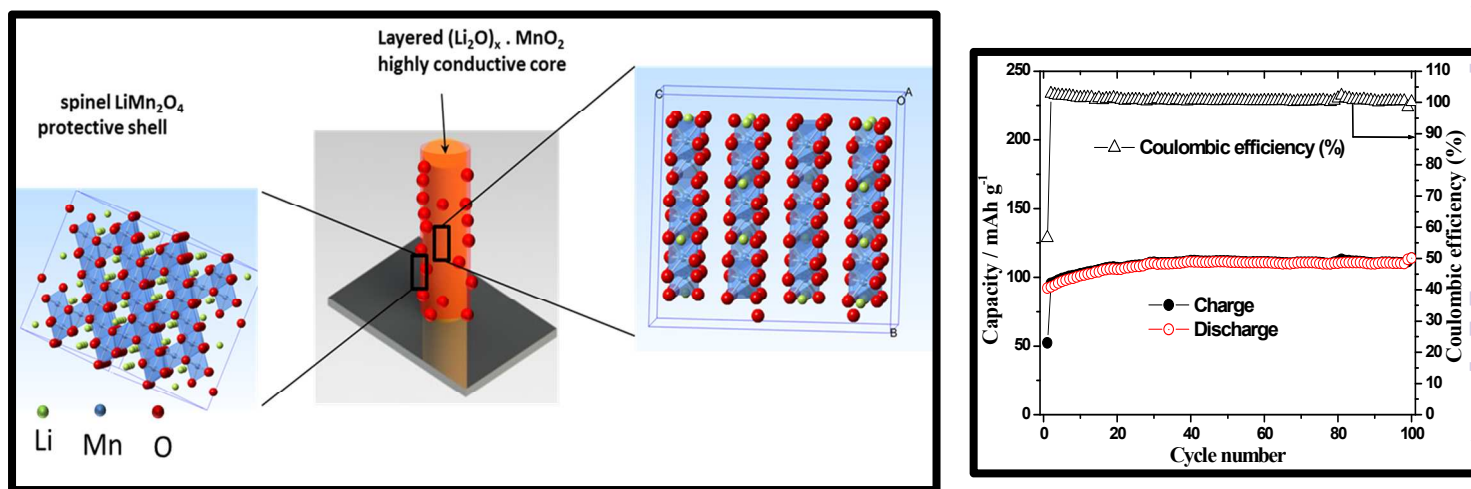


Figure: Schematic (on the left) showing LiMn_2O_4 protective shell on $(\text{Li}_2\text{O})_x \text{MnO}_2$ NWs with layered structure. Graph (on the right) showing high capacity retention and high columbic efficiency with this architecture after 100 cycles.